Vol. 18, No. 2 (2019) 463-476
Revista Mexicana de Ingeniería Química

THERMODYNAMIC STABILITY OF PROMOTED NIOBIUM SULFIDE CATALYST FOR HYDRODESULFURIZATION: A DFT STUDY

ESTABILIDAD TERMODINÁMICA DE CATALIZADORES DE SULFURO DE NIOBIO PROMOVIDOS PARA HIDRODESULFURIZACIÓN

M. Cornejo[1,4*], H. Baykara[1,4], A.B. Vidal[1,2], D. Arroyo[1], D. Zambrano[1,3], P. Iza[1,3], S. Samaniego[1], A. Martiz[1], E.V. Ludeña[1,5]

[1] *Center of Nanotechnology Research and Development, CIDNA, Escuela Superior Politécnica del Litoral, ESPOL, Km 30.5 vía Perimetral, Campus G. Galindo, Guayaquil, Ecuador.*
[2] *Laboratory of Chemical Physics and Computational Catalysis, IVIC, Apartado 21827, Caracas 1020-A, Venezuela.*
[3] *School of Natural Sciences and Mathematics, Department of Physics, ESPOL, Km 30.5 Via Perimetral, Campus Gustavo Galindo, Guayaquil Ecuador.*
[4] *Faculty of Mechanical Engineering and Production Science, ESPOL, Km 30.5 via Perimetral, Campus Gustavo Galindo, Guayaquil, Ecuador.*
[5] *Laboratory of Theoretical Physical Chemistry of Materials, IVIC, Apartado 21827, Caracas 1020-A, Venezuela.*

Received: December 01, 2018; Accepted: January 31, 2018

Abstract

Density functional theory calculations of single-layer models of niobium sulfide catalysts promoted at the S-border by the transition metal atoms V, Cr, Fe, Co, Ni, and also by Cu are performed. Different degrees of promotion as well as of sulfidation are studied. The canonical potential for the sulfidation reaction for these models is obtained and the thermodynamic stability of these catalysts in terms of composition, temperature and pressure (pH_2S/pH_2) is examined. At working conditions (T=650K and pH_2S/pH_2=0.05) the most stable catalysts correspond to $100V75S$ and $100Cr100S$ which are structures where the promoter atoms fully replace the Nb atoms at the upper row of the single-layer crystal at the S-border. The potential activity of the active sites in these catalysts was studied by means of the surface electrostatic potential, $V_S(\mathbf{r})$. The implications for the HDS reaction in hydrotreating conditions of these novel catalyst models are discussed.

Keywords: *DFT*, Canonical Potential, Promotor effect, Niobium Sulfide Catalysts, HDS.

Resumen

Se realizaron cálculos utilizando la teoría del funcional de la densidad de modelos de catalizadores de capa-única de sulfuro de niobio promovidos en el borde-S por los metales de transición V, Cr, Fe, Co, Ni, y también Cu. Se estudiaron diferentes grados de promoción al igual que de sulfuración. Se obtiene el potencial canónico para la reacción de sulfuración para estos modelos, y se examina la estabilidad termodinámica de estos catalizadores en términos de composición, temperatura, y presión (pH_2S/pH_2). En condiciones de trabajo (T=650K y pH_2S/pH_2=0.05) los catalizadores más estables son $100V75S$ y $100Cr100S$ que son estructuras donde el metal promotor reemplaza completamente los átomos de Nb en la fila superior del cristal de capa-única en el borde-S. Se estudio la actividad potencial de los sitios activos en estos catalizadores por medio del potencial electrostático superficial, $V_S(\mathbf{r})$. Se discute las implicaciones para la reacción de HDS en condiciones de hidrotratamiento de estos nuevos modelos de catalizadores.

Palabras clave: *DFT*, potencial canónico, efecto promotor, catalizadores de sulfuro de niobio, HDS.

1 Introduction

The need for refineries to provide cleaner fuels complying with stricter environmental regulations, such as the requirement that after 2011 fuel oils in the European Union must have a maximum sulfur content of 10 mg/kg certainly has placed a stringent demand on the development of more efficient hydrodesulfurization (HDS) processes. This demand, in turn, has promoted much research in the design, synthesis and characterization of more efficient HDS catalysts (Costa *et al*., 2013; Torres, 2018).

* *Corresponding author. E-mail*: mcornejo@espol.edu.ec
https://doi.org/10.24275/uam/izt/dcbi/revmexingquim/2019v18n2/Cornejo
issn-e: 2395-8472

Essentially these improvements can occur due to changes in the active component, variations in the methods of preparation and developments related to structure and properties of the support (Okamoto *et al*., 2005; Romero *et al*., 2019).

For the HDS of oils and derivatives, the standard catalysts have traditionally comprised combinations of $Co(Ni)MoS$ compounds supported and dispersed over a variety of materials (Costa *et al*., 2013; Song *et al*., 2015). But the presence of refractory organosulfur compounds such as alkyl-dibenzothiophene, in addition to thiophene, in the heavy oil loads which need to be processed nowadays, has fostered the search for improvements on traditional catalysts (Humbert *et al*., 2016).

Alternatives to the standard $NiCo-MoS$ catalysts have a long history. In the 70s and 80s it was already known that the addition of small amounts of niobium oxide and tantalum oxide enhanced the activity and selectivity of many standard catalysts and even improved their stability (Eijsbouts *et al*., 2013; Ushikubo, 2000). We consider in this work niobium sulfide as an alternative to MoS_2. The reason is that among the pure transition metal sulfides (non-promoted) niobium sulfides and MoS_2 have significant catalytic activities (0,8-2,3) for hydrodesulphurization (HDS) reactions. According to the data in the literature it can be said that there is a correlation between electronegativity of the mixed metal sulfides and HDS activity (Afanasiev *et al*., 2007).

Even though NbS_2 has a low surface area; its catalytic activity is very high when it is used for the isomerization and hydrogenation of 1-butene. Unsupported niobium sulfides (NbS_3, NbS_2, a non-stoichiometric disulfide, Nb_{1+xS2}) have been used in different applications such as hydrotreatment (hydrodesulfuzation, hdyrodenitrogenation, and hydrogenation) reactions. Especially in cleavage of $C-N$ and $C-C$ bonds and high selectivity in hydrogenation reactions, niobium sulfides have catalytic activities remarkably better than those of molybdenum disulfide. Niobium sulfides show different activities depending on the preparation technique and the nature of the supporting material. One of the reasons of different catalytic activities is dispersion of the catalyst on the support. It has been found, for example, that MoS_2 attaches to the specific regions on the surface of support in a monolayer dimension, and the maximum catalytic activity is found at a 10% (w/w) Mo load (Afanasiev *et al*., 2007).

Sulfides of molybdenum and niobium have potential use in applications such as optoelectronics, microelectronics, solar cell elements, nano tribology and catalysis. Since MoS_2 and niobium sulfides have layered structures they can be exfoliated to obtain new particles with different thickness up to single layers. Cleavage of the lamellar structure of NbS_2 along the plane (100) produces surface models exposing coordinatively unsaturated niobium at one edge and sulfur atoms at the other. In a previous work (Aray *et al*., 2014a), we have carried out a density functional theory and first-principles surface thermodynamics calculations at hydrodesulfurization conditions for the metal-edge of pure NbS_2 catalyst mixed with Mo and promoted with V, Fe, Co,, and Ni. In that study the emphasis was placed on the metallic edge reactivity when it was promoted by Co or Ni atoms. In addition, the canonical potential for the gas phase mixture (H_2+H_2S) was evaluated at the metallic edge for an activated mixed catalysts of the type $Nb_2Mo_3S_{10}$.

One of the suppositions underlying the work of Aray *et al*. (2014), is that the number of coordinatively unsaturated sites (CUS) on the edges of the active phases correlates with the catalytic activity for HDS. Thus, the activity is higher when more vacant sites are present. However, there is experimental evidence that fully sulfided Mo catalysts, namely, catalysts having the lowest number of CUS, evince, nonetheless, the highest thiophene HDS activity. This finding implies that the presence of CUS is not a determinant factor for thiophene HDS (Vogelaar *et al*., 2009). In addition, Drescher *et al*. (Isomerization *et al*., 2012) have shown that hydrogenation and cis-trans isomerization can be explained without having to resort to CUS. Hydrogenation of unsaturated molecules occurred, according to XPS analysis in surface states saturated by sulfide species.

More recently, Lauritsen and Besenbacher (2015) have advanced an interpretation of how bright brim sites work which does not rely on CUS. The claim based on direct STM observations is that aromatic molecules are adsorbed in a flat lying configuration. Hydrogenation takes place through the interaction with $S-H$ groups located at the nanoparticle edges of single layer MoS_2 and $CoMoS$ structures. Thus, according to this interpretation, hydrogenation occurs because of the interaction of aromatic pi systems with the metallic edge states of bright brim sites. One of the conclusions of Vogelaar *et al*. (2009), is that for Mo and $NiMo$ HDS catalysis the thiophene and the dibenzothiophene hydrogenation pathways proceed through interaction with sulfided species on the active

phase. There is some recent experimental evidence indicating that for single-layer MoS_2 nanocrystals, Co,-promoter atoms attach preferentially at the S-edge termination. Moreover, they are absent at the Mo-edge termination (Zhu *et al*., 2016).

In the present work, we determine the canonical potential for the case of single-layer models of niobium sulfide catalysts promoted by a number of transition metals such as V, Cr, Fe, Co, Ni, and also by Cu. To this purpose, we perform DFT calculations of these catalyst models. An important improvement on the previous calculation of Aray *et al*. (2014b) has to do with the inclusion of dispersive effects in the DFT application. We study the sulfidation reaction at the S-border for different degrees or promotion at the terminal Nb row of a single-layer structure as well as different degrees of sulfidation. We examine the thermodynamic stability conditions dependent on composition, temperature and the relative pH_2S/pH_2 pressure for this sulfidation reaction. We also calculate the electrostatic potential $V_S(\mathbf{r})$ at $\rho(\mathbf{r}) = 0.001$ in order to determine the nature of the active sites available for the HDS reaction.

2 Materials and methods

2.1 DFT calculations

Theoretical calculations were performed using the DMol^3 code with numerical atomic functions (Delley, 1990, 2000). The general gradient approximation with the Perdew-Burke-Ernzerhof functional ($GGA-PBE$) (Kurth *et al*., 1999; Perdew *et al*., 1996) was used to treat the electronic structure, and the basis set was represented by the double numerical plus polarization (DNP) basis. In particular, the Grimme method (Grimme, 2006) was employed for dispersion corrections ($DFT-D$ correction). This method has shown to be reliable for studying the binding properties of various layered solids (Bučko *et al*., 2010). To improve the calculation speed, effective core potentials were used to represent the core electrons and spin polarization scheme was applied to all calculations. The orbital cutoff was 5.0 Å. A Monkhorst-Pack (Monkhorst *et al*., 1976) mesh k-point of $(1 \times 1 \times 1)$ was used because of the large supercell. A. vacuum layers thicker than 15 Å were used to ensure that there were no interactions between adjacent slabs. In the present work, the vibrational contribution for all studied surface models, bulk models, and H_2S and H_2 molecules were also included.

2.2 Surface models

NbS_2 is a layered transition metal dichalcogenide with a structure similar to that of MoS_2 bulk (space group $P6_3/mmc$). The calculated lattice parameter of the cell is $a = b = 3.349$ Å and $c = 12.204$ Å, in reasonably good agreement with the experimental values ($a = b =$ 3.310Å, $c = 11.890$ Å) (Jellinek *et al*.,1960). In order to check the influence of the $DFT-D2$ correction on the lattice parameters of bulk NbS_2, we performed the calculation with GGA only and found that a changes less than 2% while c increases by as much as 9% with respect to the experimental value. Cleavage of the NbS_2 bulk structure parallel to the 100 plane produces the edge surface models exposing two well-known kinds of MoS_2- like catalysts edges: the M-edge and the S-edge. Our model for the NbS_2 surface is shown in Fig. 1.

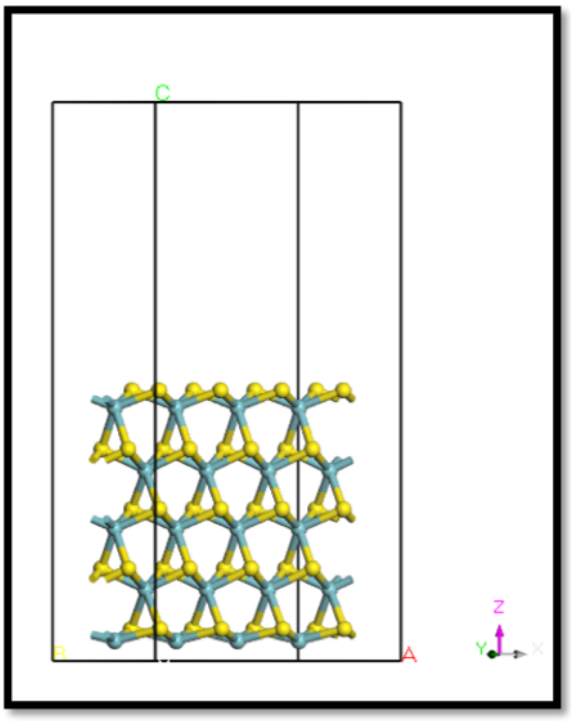

Fig. 1. Periodic slab used to simulate the S-edge of NbS_2 single-layer crystal. Yellow and green spheres denote the S and Nb atoms, respectively.

It consists of infinite monolayer model which exposes both the S-edge (at the top) and the Nb-edge (at the bottom). This model is consistent with experimental findings on the morphology of MoS_2 clusters under a H_2S/H_2 environment (Lauritsen *et al.*, 2015). We use a supercell consisting of five $S-Nb-S$ rows in the z-direction and four $S-Nb-S$ units in the y-direction so that four nonequivalent Nb surface sites are present. The total supercell of the stoichiometric monolayer contains a $Nb_{40}S_{20}$ unit within a volume of 13.397Å× 12.204Å× 29.503Å (Fig. 1).

The promotion effect brought about by the substitution of Nb atoms at the S-edge by V, Cr, Fe, Co, Ni and is studied in the present work. Previously (see Aray *et al.*, 2014b) we had explored the case of a partial (50%) and full (100%) substitution of Nb atoms at the Nb-edge by the promoter atoms V, Fe, Co, and Ni. Therefore, here we focus only on the S-edge taking into account the 100% of the edge outermost Nb atoms substituted by the metal promoter (Me) and the partial (50%) promoter edge content with two different distributions: either an alternated distribution ($-Nb-Me-Nb-Me-$), or a paired distribution ($-Nb-Nb-Me-Me-$), as reported by previous DFT calculations for the MoS_2 monolayer promoted with Ni and Co (Krebs *et al.*, 2008). For the unpromoted and promoted S-edge, we considered sulfur coverages of 37.5, 50, 62.5, 75 and 100%.

2.3 Surface thermodynamics

In order to evaluate the surface stability at different temperature, partial pressure, and elemental compositions, we use the formalism of *ab initio* atomistic thermodynamics (Reuter *et al.*, 2001, 2003). On the basis of this method, the stabilities and properties of several transition metal oxides (Reuter *et al.*, 2002; Rogal *et al.*, 2004), sulfides (Aray *et al.*, 2009; Aray *et al.*, 2009; Aray *et al.*, 2014b), carbides (Wang *et al.*, 2011; Zhao *et al.*, 2012), and phosphides (He *et al.*, 2016) have been reported. The stability of a given surface can be determined by calculating the canonical potential $\Omega(T,p)$, at temperature T and partial pressure p of the gas phase components. The general thermodynamic formula for $\Omega(T,p)$ is

$$\Omega(T,p) = G - \sum_i N_i \mu_i(T,p) \tag{1}$$

where, G stands for the Gibbs free energy of the surface which is modelled by a piece of material (slab) in a grand canonical ensemble at constant temperature T and total pressure p. $\mu_i(T,p)$ is the chemical potential of the various species i present in the system, and N_i gives the number of atoms of the i$-th$ component contained in the solid slab model. Therefore, the canonical potential, $\Omega(T,p)$, of a NbS_2 surface can be written as

$$\Omega(T,p) = G^{slab}_{Nb_xS_y} - x\mu_{Nb}(T,p) + y\mu_S(T,p) \tag{2}$$

where $G^{slab}_{Nb_xS_y}$ is the total Gibbs free energy of the slab, containing x niobium atoms and y sulfur atoms, and μ_{Nb} and μ_S are the chemical potentials of Nb and S atoms, respectively. The chemical potentials μ_{Nb} and μ_S are connected through bulk NbS_2, which serves as reservoir of Nb atoms. Thus, we have

$$\mu_{Nb} + 2\mu_S = g^{bulk}_{NbS_2} \tag{3}$$

$g^{bulk}_{NbS_2}$ is the total Gibbs free energy of NbS_2 crystal structure per formula unit. Inserting Eq 3 into Eq 2 the canonical potential of the slab becomes a function of the μ_S, therefore

$$\Omega(T,p) = G^{slab}_{Nb_xS_y} - xg^{bulk}_{NbS_2} + (2x-y)\mu_S(T,p) \tag{4}$$

$$\mu_S = \mu_{H_2S} - \mu_{H_2} \tag{5}$$

The term $(2x-y)$ stands for the excess or lack of sulfur atoms compared to the bulk stoichiometry. Negative values correspond to excess sulfur, whereas positive values are related to sulfur deficiencies. μ_S is determined by the chemical equilibrium with the gas-phase mixture ($H_2 + H_2S$).

The Gibbs free energy is associated with the Helmholtz free energy, F, via

$$G(T,p,x,y) = F(T,p,x,y) + pV(T,p,x,y) \tag{6}$$

In general, the F can be written as

$$F(T,V,x,y) = E^{total}_{DFT}(V,x,y) + F^{vib}(T,V,x,y) \tag{7}$$

with

$$F^{vib}(T,V,x,y) = E^{vib}(T,V,x,y) - TS^{vib}(T,V,x,y) \tag{8}$$

Here E^{vib} and S^{vib} are the vibrational energy (including the zero-point energy) and entropy, respectively. The pV term is negligible (Reuter *et al.*, 2002) ($\sim 10^{-3}$ meV/Å^2) compared to the F free energy. Thus, the only additional contributions to the

surface Gibbs free energy apart from the *DFT* total energy are the vibrational terms,

$$E^{vib} = \frac{R}{k}\frac{1}{2}\sum_i h\nu_i + \frac{R}{k}\sum_i \frac{(h\nu_i)e^{(-h\nu_i/kT)}}{[1-e^{(-h\nu_i/kT)}]} \quad (9)$$

$$S^{vib} = R\sum_i \frac{(h\nu_i/kT)e^{(-h\nu_i/kT)}}{[1-e^{(-h\nu_i/kT)}]} - R\sum_i \ln\left[1-e^{(-h\nu_i/kT)}\right] \quad (10)$$

In practical calculations, the chemical potential of the gas phase mixture ($H_2 + H_2S$), is evaluated using the general thermodynamic formula assuming ideal gas behavior

$$\mu_S = \Delta E_{el} + \Delta ZPE + \Delta H(T) - T\Delta S(T) + RT\ln\left(\frac{pH_2S}{pH_2}\right) \quad (11)$$

here, $\Delta H(T)$ and $\Delta S(T)$ stand for enthalpy and entropy differences, respectively, at T for H_2S and H_2, and ΔE_{el} for the difference of their internal energies $[E_{el}(H_2S) - E_{el}(H_2)]$, which are approximated by their zero-temperature *DFT* total energies. ΔZPE represents the zero-point vibrational energy term $[(H_{H_2S}(0) - E_{el}(H_2S) - (H_{H_2}(0) - E_{el}(H_2)]$ calculated through evaluation of the Hessian matrix elements using the normal modes analysis module implemented in the program DMol[3] .

Large values of μ_S correspond to sulphur-rich conditions, whereas small values of μ_S relate to strongly reducing conditions, in which hydrogen is more abundant than H_2S in the gas phase.

For the surfaces promoted with metal (Me) atoms (V, Cr, Fe, Co, Ni and Cu) and with composition $Me_zNb_xS_y$ the canonical potential is given by;

$$\Omega(T,p) = G^{slab}_{Me_zNb_xS_y} - xG^{bulk}_{NbS_2} - \frac{z}{a}G^{bulk}_{Me_aS_b} + \left(2x + \frac{b}{a}z - y\right)\mu_S(T,p) \quad (12)$$

where $G^{slab}_{Me_zNb_xS_y}$ is total Gibbs free energy of the promoted slab, containing x niobium atoms, y sulfur atoms and z promoter atoms, and $G^{bulk}_{Me_aS_b}$ is the total Gibbs free energy of the promoter bulk phase (VS, Cr_3S_2, FeS_2, Ni_3S_2, Co_9S_8, CuS) stable in reaction conditions. The term $\left(2x+\frac{b}{a}z-y\right)$ stands for the excess (or lack) of sulfur atoms in the slab with respect to the stable monosulfide phases.

3 Results and discussion

3.1 Determining the stable S-edge structures

Table 1 shows the binding energy values calculated for the different border structures of the promoted catalysts. The most energetically favorable structures with the same number of atoms but different border arrangement to carry out the thermodynamic stability analysis have been selected. The analysis basically depends on the free energy of the system as a function of temperature and the ratio of the partial pressures for H_2S and H_2.

3.2 S-border structure models of niobium sulfide (NbS2) catalyst promoted with a metal (Me=V, Cr, Fe, Co, Ni, Cu)

The S-border structure models were generated through the substitution of promoter atoms at the top border of the periodic slab shown in Fig. 1. The nomenclature used to identify these structures is $XMeYS$, where X indicates the percentage of replacement by Me atoms and Y, the percentage of sulfidation over the border. Thus, when the 4 Nb atoms at the upper border have been substituted, X=100, When only 2 have been substituted, X=50. Of course, in the case of a two-atom substitution, there arises two situations corresponding to the case of neighboring (paired) and alternating substituents. As on each of the border metallic atoms, at most 2 sulfur atoms can be placed, we have that a Y=100 value (100%S sulfur coverage) implies the presence of 8 sulfur atoms. The distribution of these sulfur atoms on the border metallic atoms is given by ($n_1n_2n_3n_4$) where n_i is the number of sulfur atoms over the "I" atom (the value of "I" increases from left to right). In this nomenclature, when the sulfur atoms are shared, the occupation number n_i corresponds to the sulfur atoms left of the "i" atom.

In Fig. 2, we present the different structures corresponding to a total X=100 replacement of the upper border Nb atoms. The sulfur atom coverage, described by Y, spans values of Y=100 with structure (2222), Y=75 (1212) and (2220), Y=50 (1111) (linear bridge), (1111) (seesaw bridge) and (2020) (dimer pair), and finally, Y=37.5 with structure (0102).

Table 1. *DFT* binding energies (in eV) calculated for several border structures of niobium sulfur (NbS_2) catalyst promoted with a metal ($Me = V, Cr, Fe, Co, Ni, Cu$).

Structure	Energy (eV)					
	Cu	*Fe*	*V*	*Cr*	*Ni*	*Co*
100% Me						
100Me 100S	-292.67	-309.03	-318.14	-304.32	-308.39	-310.34
100Me 75S	-285.55	-301.54	-310.79	—	-302.5	-304.16
100Me 75S+	—	—	-308.72	—	—	—
100Me 62.5S	-283.65	—	—	—	—	—
100Me 50S bridge	-278.8	-294.3	-303.1	—	-294.59	-296.53
100Me 50S Bridge+	—	—	-298.55	—	—	—
100Me 50S dimer	-280.16	—	-299.16	—	-295.73	-295.04
100Me 37.5S	-276.58	—	—	—	—	—
50% Me Pairing						
50Me 100S	-305.38	-313.94	-318.42	-311.28	-313.62	-314.73
50Me 75S bridge	—	-305.11	-310.05	-302.73	-305.62	-306.47
50V 75S bridge +	-299.31	-306.17	-310.72	-303.56	-307.25	-307.67
50Me 75S dimer	-299.47	-305.46	-303.86	-302.32	-307.57	—
50Me 62.5S +	—	-302.6	-296.3	-299.77	-303.59	-304.17
50Me 62.5S New	-295.62	—	—	—	—	—
50Me 62.5S	-294.4	-300.5	-304.58	-298.64	-302.4	—
50Me 62.5S New+	—	—	-306.94	—	—	—
50Me 50S bridge	-292.06	-298.63	-303.02	-295.95	-299.61	-300.1
50Me 50S dimer	-289.79	-295.71	-299.14	-292.64	-297.75	-297.23
50Me 37.5S	-288.675	—	—	—	—	—
50% Me Alternated						
50Me 100S	-304.98	-313.93	-318.26	-311.45	-313.18	-314.46
50Me 75S	-298.33	-306.65	-308.44	-303.67	-307.84	-308.15
50Me 62.5S	-296.44	-302.61	-304.57	-299.98	-303.2	-304.3
50Me 50S bridge	-293.07	-298.37	-303.01	-296.22	-299.98	-300.33
50Me 50S dimer	-287.65	-294.04	-298.48	-292.46	-297.08	-297.32

The S-border structures corresponding to X=50% where the replaced neighbor atoms are paired are shown in Fig. 3. As we can see in this figure, there is a single structure with Y=100% S coverage (2222). A sulfur coverage of Y=75% corresponds to 6 sulfur atoms placed over the metal ones. This gives rise to the structures (2121), (1212), (2002) and (2220). When there are 5 sulfur atoms, the coverage is Y=62.5% and the structures are (1121), (2111), (1202) and (1220). A Y=50% corresponds to the distributions of 4 atoms giving rise to the structures (1111) and (2020). Finally, when there are 3 sulfur atoms Y=37.5% and the structure is (1011). Similarly, in Fig 4 we present the ball and rod models of structures corresponding to an X=50% replacement of the promoter atoms but where the replacing atoms occupy alternating sites. As in the previous case there arise a number of different border structures due to different sulfur coverage. In the present case, we have included only the most stable structures. For a sulfur coverage of Y=100% we have the border structure (2222). For Y=75% the structures are (2121) and (2220). For Y=67.5% sulfur coverage, we have the structures (1121) and (1220). Finally, for Y=50% we have the structures (1111) and (0202).

3.3 *Canonical potentials of promoted catalyst models*

An important issue, having direct relevance to the nature of the active sites is the study of the $H_2 - H_2S/Me_zM_yS_x$ gas-solid interface.

Case I. 100% Me substitution

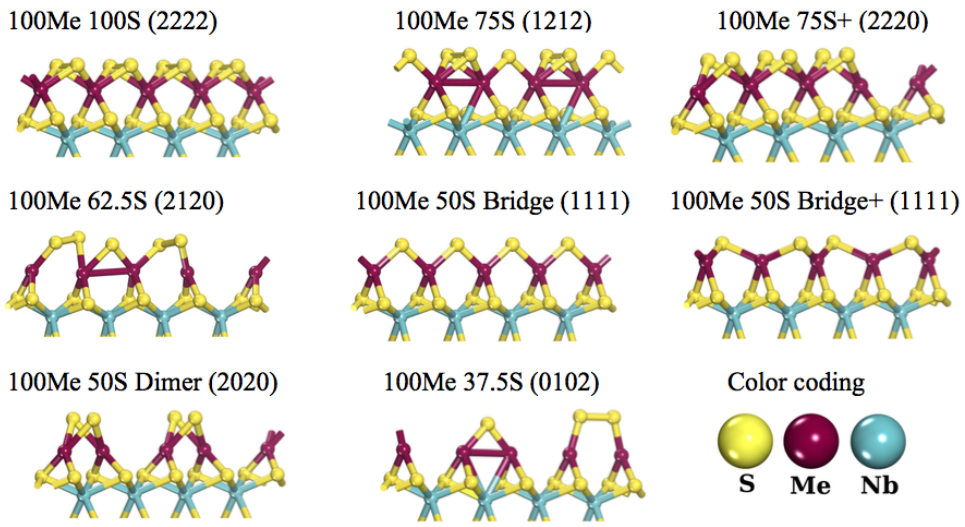

Fig. 2. Ball and rod models of the *S*-border structures generated by a 100% replacement of the upper Nb layer in the slab model of Fig. 1 by Me atoms for different coverage of sulfur atoms. Note that for 75%S, two different structures arise. In the case of 50%S coverage, we observe the appearance of three different structures bridge, bridge+ and dimer. The color code for atoms is: Yellow = sulfur (*S*), red = Promoting metal (*Me*), Blue = Niobium (*Nb*).

Case II. 50% Me paired substitution

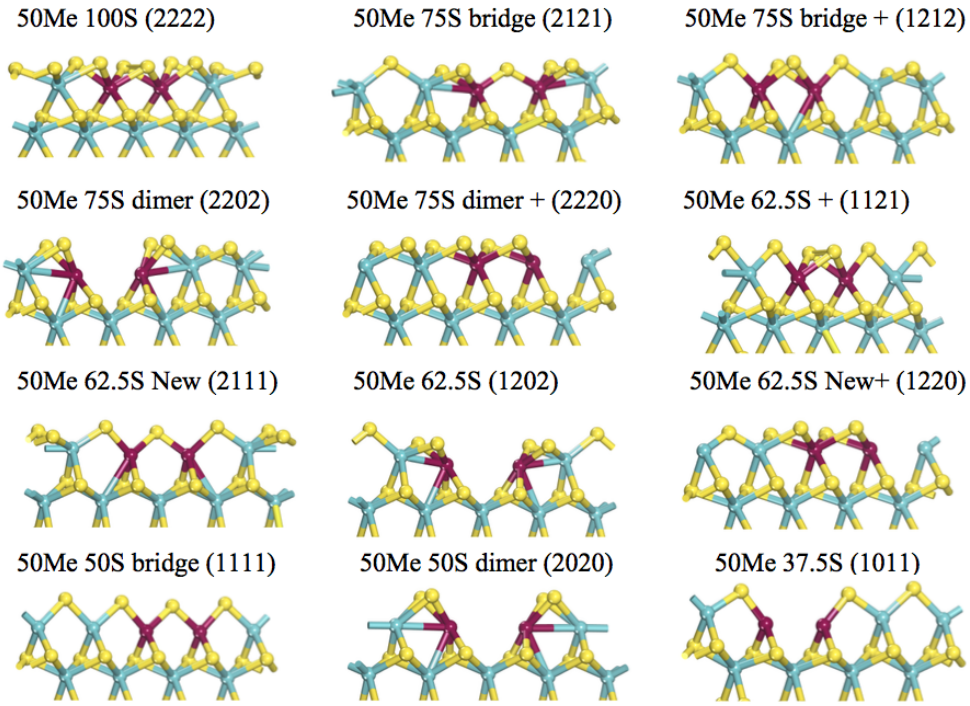

Fig. 3. Ball and rod models of the *S*-border structures generated by a 50% replacement of the upper *Nb* layer in the slab model of Fig. 1 by Me atoms for different coverage of sulfur atoms. The substituted Me atoms are placed at neighboring sites (paired). The color coding is the same as in Fig. 2.

Case III. 50% Me alternating substitution

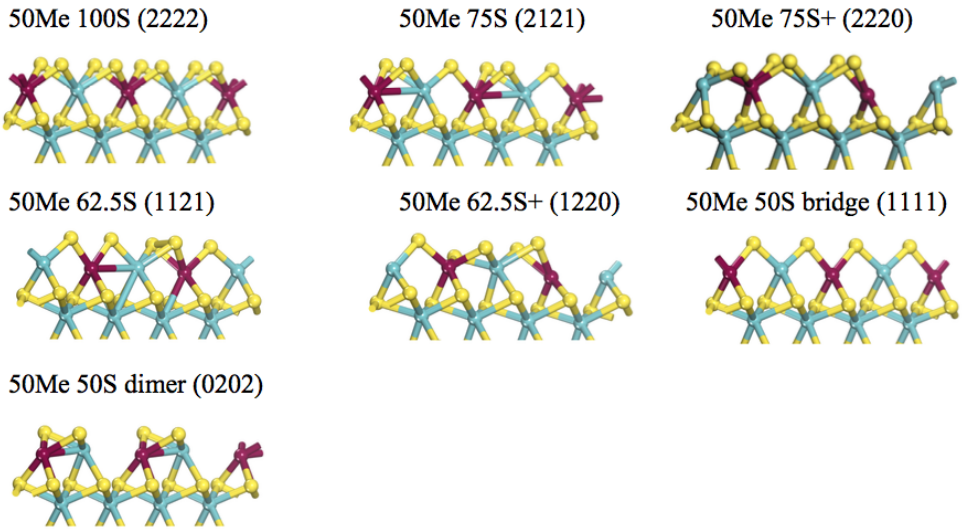

Fig. 4. Ball and rod models of the S-border structures generated by a 50% replacement of the upper Nb layer in the slab model of Fig. 1 by Me atoms for different coverage of sulfur atoms. The substituted Me atoms alternate with the Nb atoms. The color coding is the same as in Fig. 2.

For MoS_2, for example, this study was carried out by Raybaud *et al*. (Raybaud *et al*., 2000). Thus, a main objective of the present work is to examine the stability of the promoted NbS_2 catalyst S-border structures under working refinery conditions in order to assess the influence of the promoters on the catalytic process. The promoters examined are V, Cr, Fe, Co, Ni and Cu. For this purpose, we undertake the thermodynamical analysis of the reactions of the catalyst S-border atoms with H2 and H2S gases which is shown in section 2. These results have been presented in terms of graphical displays of the canonical potentials $\Omega(T, pH_2S/pH_2)$ obtained in the present DFT calculations. These canonical potentials are given as functions of the temperature and the pressure ratio pH_2S/pH_2. For the present calculations the temperature was set at the working value of T=650K.

As an example, we present in Fig. 5 graphs of the stability behavior of $\Omega(T, pH_2S/PH_2)$, measured in units meV/Å^2, corresponding to the border structures promoted by V. We can see in this figure that the catalysts present different behaviors at different pressure ranges. The overall most stable structure at T=650K and both at low and high H_2S/H_2 pressures corresponds to $100V50S$-bridge (1111) alternated one. When the pressure ratio increases the stable structure still in the low-pressure region is $100V75S$.

For the high-pressure range, the most stable structure is $100V100S$. Note that all these lines lie below the value of 12 meV/Å^2.

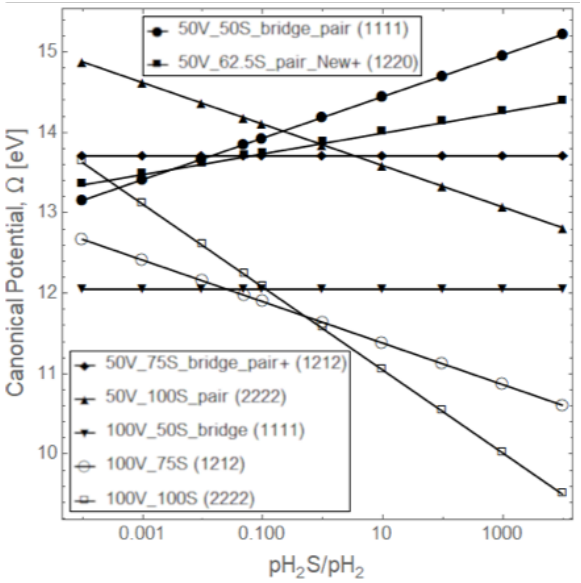

Fig. 5. Comparison of the grand canonical potentials obtained for the least-energy catalyst S-border structures of niobium sulfide promoted with vanadium. The temperature is T=650K. The graph presents the grand canonical potential as a function of ln (pH_2S/pH_2).

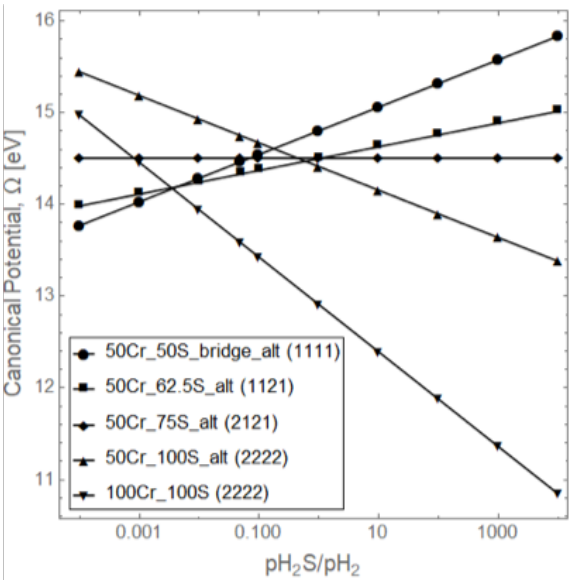

Fig. 6. Comparison of the grand canonical potentials obtained for the least-energy catalyst border-structures of niobium sulfide promoted with chromium. The temperature is T=650K. The graph presents the grand canonical potential as a function of ln (pH_2S/pH_2).

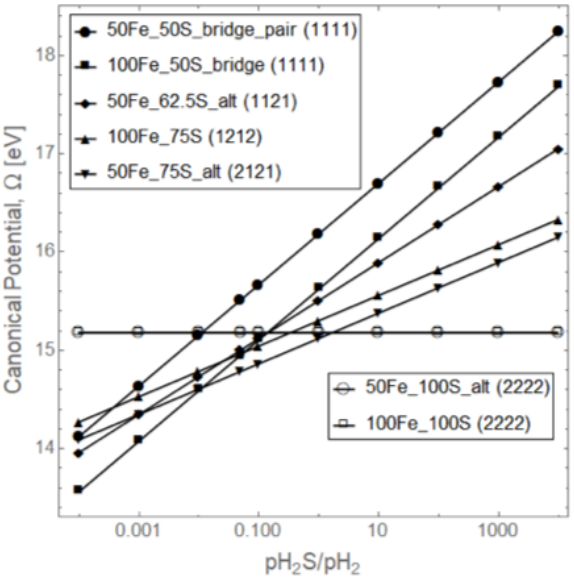

Fig. 7. Comparison of the grand canonical potentials obtained for the least-energy catalyst border-structures of niobium sulfide promoted with iron. The temperature is T=650K. The graph presents the grand canonical potential as a function of ln (pH_2S/pH_2). Notice that there is an overlapping of the $100Fe100S$ structure with the $50Fe100S$_alt structure.

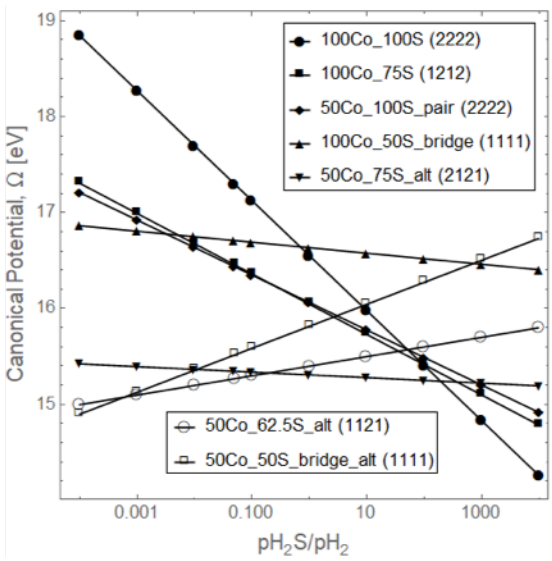

Fig. 8. Comparison of the grand canonical potentials obtained for the least-energy catalyst border-structures of niobium sulfide promoted with cobalt. The temperature is T=650K. The graph presents the grand canonical potential as a function of ln (pH_2S/pH_2).

In Fig. 6 we present the behavior of the canonical potential for the S-border structure of NbS_2 promoted by Cr. In the low pressure region, the most stable structure is $50Cr50S$-bridge-alt. At higher pressures there is a shift, however, to the structure $100Cr100S$. Similarly, in Fig. 7 we present the canonical potentials for the S-border structures promoted by Fe. We can see that the catalysts present different behavior at different pressure ranges. There are three main structures: $100Fe50S$ Bridge for low pressures of H_2S/H_2, $50Fe75S$-alt for the working range, and $50Fe100S$-alt for high pressure ratios. The lowest values of the canonical potential for the S-border structures promoted by Co are presented in Fig 8. These lowest values change with increasing ratio of pH_2S/pH_2, and correspond, respectively to $50Co50S$-bridge-alt, $50Co62.5S$-alt, $50Co75S$-alt, and $100Co100S$. The behavior of Ni-promoted S-border structures of the catalyst is depicted in Fig 9. Again, we observe that there are several structures which alternate as the most stable ones when the pressure ratio pH_2S/pH_2 is increased. These structures are in consecutive order: $50Ni50S$-bridge-alt, $100Ni50S$-dimer, $100Ni75S$ and $100Ni100S$. In Fig. 10 we present graphs of the stability behavior of $\Omega(T, pH_2S/pH_2)$ corresponding to the S-border structures promoted by Cu. We can see in this figure that the catalysts present different behaviors at different pressure ranges.

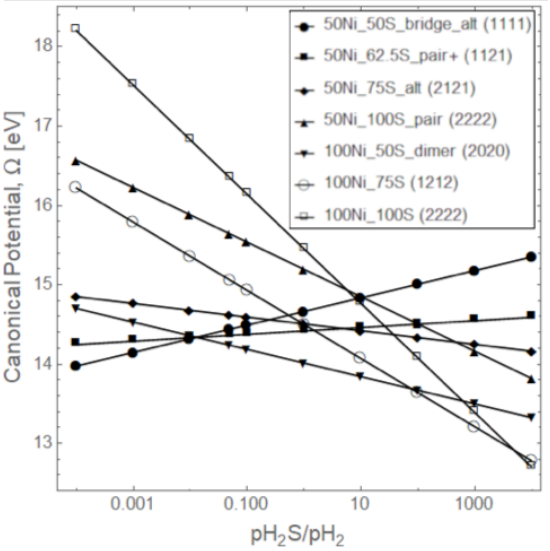

Fig. 9. Comparison of the grand canonical potentials obtained for the least-energy catalyst border-structures of niobium sulfide promoted with nickel. The temperature is T=650K.

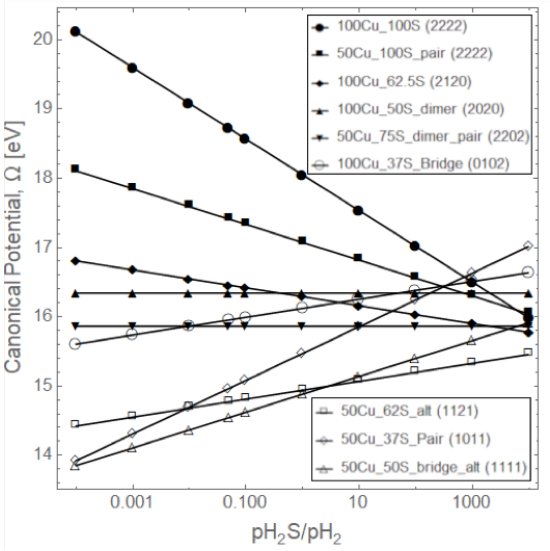

Fig. 10. The behavior of the grand canonical potential at the working temperature T=650K and as a function of (pH_2S/pH_2) obtained for the least-energy catalyst S-border-structures of niobium sulfide promoted with copper.

The overall most stable structure at T=650K at low H_2S/H_2 pressure corresponds to $50Cu50S$-Bridge (1111) alternated one. The stable structure in the high-pressure range is $50Cu62.5S$-alt.

3.4 *Promoter effect*

Comparison with promoted MoS_2 catalysts

In Fig. 11, we present the combined results of thermodynamical stability analysis for V, Cr, Fe, Co, Ni and Cu. These lines were selected as the lowest ones obtained at the refinery working conditions of 650K and at pH_2S/pH_2= 0.05. These results show the stabilizing effect of vanadium and chromium as effective promoters for the niobium sulfide catalyst.

In order to examine the stability of promoted catalysts at other refinery conditions, we have calculated the behavior of the most stable structures selected at a temperature T=650K and at pH_2S/pH_2=100. It is seen that also at these working conditions the most stable catalysts are those promoted by Cr and V.

3.5 *Determining the nature of the active sites*

3.5.1 *Electrostatic potential analysis*

In order to gain insight on the nature of the active sites in the catalyst, we resort to the study of the electrostatic potential of vanadium promoted niobium sulfide catalysts.

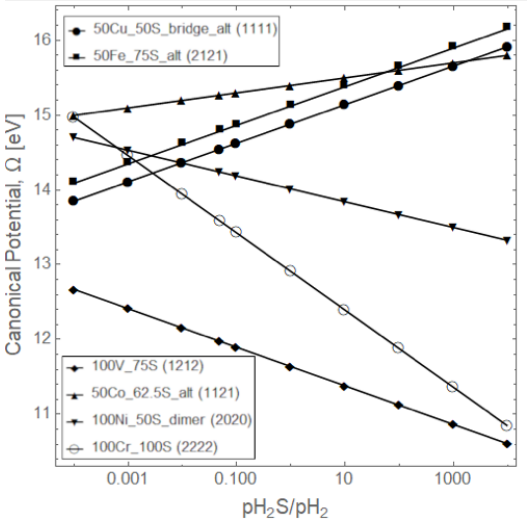

Fig. 11. Comparison of the grand canonical potentials obtained for the least-energy catalyst S-border-structures of niobium sulfide promoted with vanadium, chromium, iron, cobalt, nickel and copper. Only the most stable structure for each kind of promoter, selected at a temperature T=650K and at pH_2S/pH_2=0.05 (working refinery conditions) is shown.

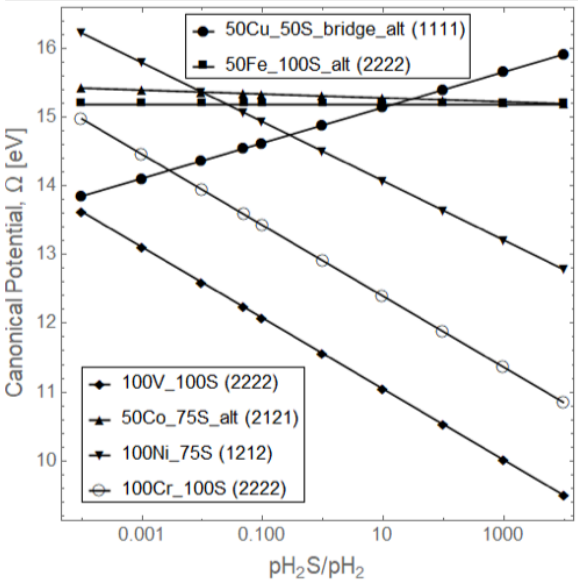

Fig. 12. Comparison of the grand canonical potentials obtained for the least-energy catalyst S-border-structures of niobium sulfide promoted with vanadium, chromium, iron, cobalt, nickel and copper. However, in contrast to the results shown in Fig. 11 the structures were selected for the minimum at pH_2S/pH_2=100.

We compare the results of $V_S(\mathbf{r})$ for $MeMoS_2$ with those of the present study, namely, $MeNbS_2$. The electrostatic potential $V(\mathbf{r})$ is a function of three dimensional space vector r and is directly derivable from electrostatics (Scrocco *et al.*, 1978; Sjoberg *et al.*, 1990). It may also be obtained from experimental results and hence, as is the case with the density $rho(\mathbf{r})$, it is a bona fide variable for the calculation of the molecular electronic structure (Theophilou *et al.*, 2005). Moreover, it is related to the density through the Poisson's equation.

The surface potential $V_S(\mathbf{r})$ has been used to introduce regions related to chemical reactivity. The surface potential is the value of $V(\mathbf{r})$ on the surface generated by the condition $rho(\mathbf{r})$=0.001 (van der Waal surface). Actually, the justification for relating it to chemical reactivity comes from the assumption that in chemical processes proceed through charge transfer in molecules from regions which are electron-rich to others which are electron-deficient. $V_S(\mathbf{r})$ has maxima $V_{S,max}(\mathbf{r})$ and minima $V_{S,min}(\mathbf{r})$ points. The local maxima on the molecule surface occur in regions where the potential is positive and the minima in regions where it is negative.

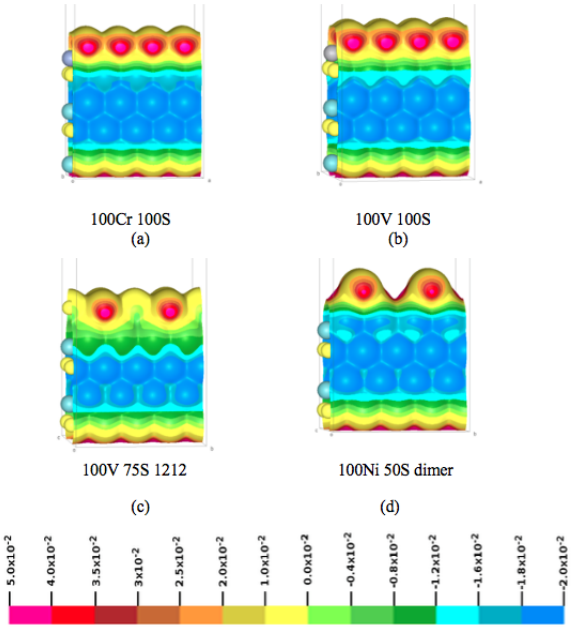

Fig. 13. Graphs of $V_{S,max}(\mathbf{r})$ for some selected lowest canonical potential structures presented in Figs 11 and 12. (a) The $100Cr100S$ structure which is the second lowest one both at pH_2S/pH_2=0.5 and pH_2S/pH_2=100 (T=650K). %(b) The $100V100S$ structure which is the lowest one at pH_2S/pH_2=100 (T=650K). (c) The $100V75S$ (1212) structure which is the lowest one at working conditions pH_2S/pH_2=0.5 (T=650K). (d) The $100Ni50S$-dimer (0202) structure which is the third lowest lying one at pH_2S/pH_2=0.5 (T=650K). The color scale defines the values of the $V_{S,max}(\mathbf{r})$ potential. Notice that the most positive values are located at the S-border atoms.

The former is related to acid sites and the latter to basic ones. It has been determined (Sjoberg *et al.*, 1990) that in covalently bonded atoms there are regions of $V_{S,max}(\mathbf{r})$ (denoted as sigma(σ)-holes) where apparently there is a depletion of electronic density of the orbital forming the sigma bond (Halldin *et al.*, 2018). Thus, a halogen bond, for example, is an electrostatically driven interaction taking place between a positive sigma-hole and a region of negative potential. Bond formation takes place by an electron density transfer between a Lewis base, acting as an electron donor, and a Lewis acid, acting as an electron acceptor (Mohan *et al.*, 2014).

The extension of these concepts to determine the reactivity of compounds containing transition metal atoms, such as the catalysts structures considered here, is not straightforward. In a recent work, it has been

found that the maxima of $V_S(\mathbf{r})$, (σ-holes) are either localized or diffuse. However, for H_2O adsorption, the maxima of $V_S(\mathbf{r})$ can be related to O-down adsorption sites whereas minima in $V_S(\mathbf{r})$ leads to H-down adsorption (Halldin *et al*., 2018).

We present in Fig. 13 the results of the electrostatic potential analysis carried out for the three lowest structures at working conditions given in Fig 11 by $100V75S$ and $100Cr100S$ and $100Ni50S$ and also for the two lowest structures at high pH_2S conditions given in Fig. 12 by $100V100S$, $100Cr100S$. Note that in both cases we have $100Cr100S$ as a stable repeated structure. For the $100Me100S$ structures, we have four highly positive regions for $V_{S,max}(\mathbf{r})$ at the lateral positions of the edge sulfur atoms. Similarly, for the $100Me75S$ and $100Me50S$, we have two lateral regions for $V_{S,max}(\mathbf{r})$ associated with S-border atoms. These maxima represent sigma holes and are regions for catalysis.

Conclusions

We have studied the thermodynamic stability of the promoted niobium sulfide catalyst intervening in the $H_2 - H_2S/Me_zNb_yS_x$ gas-solid interface, where $Me = V,Cr,Fe,Co,Ni$ and Cu. We have examined the behavior of the canonical potential of the S-border promoted NbS_2 structure as a function of both the temperature and the relative pressure pH_2S/pH_2. Under working refinery conditions T=650K and pH_2S/pH_2=0.05, the most stable structures follow the order: $100V75S < 100Cr100S < 100Ni50S$-dimer $< 50Cu50S-bridge-alt < 50Fe50S-alt < 50Co62.5S$-alt. The order of the most stable structures at other refinery conditions, T=650 and pH_2S/pH_2=100 is: $100V100S < 100Cr100S < 100Nt75S < 50Fe100S-alt < 50Cu75S$-alt $< 50Cu50S$-bridge-alt.

Let us notice that in the three lowest structures in the first working conditions (T=650K and and $pH_2S/pH_2 = 0.05$) the replacement of Nb atoms by promoter atoms (V,Cr and Ni) is complete.

References

Afanasiev, P., & Bezverkhyy, I. (2007). Ternary transition metals sulfides in hydrotreating catalysis. *Applied Catalysis A: General 322(SUPPL.)*, 129-141. http://doi.org/10.1016/j.apcata.2007.01.015

Aray, Y., Vega, D., Rodriguez, J., Vidal, A. B., Grillo, M. E., & Coll, S. (2009). First-principles study of low miller index Ni_3S_2 surfaces in hydrotreating conditions. *The Journal of Physical Chemistry B 113*, 3058-3070. http://doi.org/10.1021/jp8072798

Aray, Y., Vidal, A. B., Rodriguez, J., Grillo, M. E., Vega, D., & Coll, D. S. (2009). First principles study of low miller index RuS_2 surfaces in hydrotreating conditions. *The Journal of Physical Chemistry C 113*, 19545-19557. http://doi.org/10.1021/jp809020t

Aray, Y., Zambrano, D., Cornejo, M. H., Ludeña, E. V, Iza, P., Vidal, A. B., ... Paredes, C. (2014). First-principles study of the nature of niobium sulfide catalyst for hydrodesulfurization in hydrotreating conditions. *The Journal of Physical Chemistry C 118*, 27823-27832. http://doi.org/10.1021/jp5059269

Bučko, T., Hafner, J., Lebègue, S., & Ángyán, J. G. (2010). Improved description of the structure of molecular and layered crystals: *ab initio DFT* calculations with van der Waals corrections. *The Journal of Physical Chemistry A, 114*, 11814-11824. http://doi.org/10.1021/jp106469x

Costa, V., Guichard, B., Digne, M., Legens, C., Lecour, P., Marchand, K., ... Geantet, C. (2013). A rational interpretation of improved catalytic performances of additive-impregnated dried CoMo hydrotreating catalysts: a combined theoretical and experimental study. *Catalysis Science and Technology 3*, 140-151. http://doi.org/10.1039/C2CY20553J

Delley, B. (1990). An all-electron numerical method for solving the local density functional for polyatomic molecules. *The Journal of Chemical Physics 92*, 508-517. http://doi.org/10.1063/1.458452

Delley, B. (2000). From molecules to solids with the DMol^3 approach. *The Journal of Chemical Physics 113*, 7756-7764. http://doi.org/10.1063/1.1316015

Eijsbouts, S., Anderson, G. H. H., Bergwerff, J. A. A., & Jacobi, S. (2013). Economic and technical impacts of replacing Co and

Ni promotion in hydrotreating catalysts. *Applied Catalysis A: General 458*, 169-182. http://doi.org/10.1016/j.apcata.2013.03.043

Grimme, S. (2006). Semiempirical GGA-type density functional constructed with a long-range dispersion correction. *Journal of Computational Chemistry 27*, 1787-1799. http://doi.org/10.1002/jcc.20495

Halldin Stenlid, J., Johansson, A. J., & Brinck, T. (2018). σ-Holes and σ-lumps direct the Lewis basic and acidic interactions of noble metal nanoparticles: introducing regium bonds.*Physical Chemistry Chemical Physics 20*, 2676-2692. http://doi.org/10.1039/C7CP06259A

He, J., Morales-García, Á., Bludský, O., & Nachtigall, P. (2016). The surface stability and equilibrium crystal morphology of Ni_2P nanoparticles and nanowires from an *ab initio* atomistic thermodynamic approach. *CrystEngComm 18*, 3808-3818. http://doi.org/10.1039/C6CE00584E

Humbert, S., Izzet, G., & Raybaud, P. (2016). Competitive adsorption of nitrogen and sulphur compounds on a multisite model of NiMoS catalyst: A theoretical study. *Journal of Catalysis 333*, 78-93. http://doi.org/10.1016/j.jcat.2015.10.016

Jellinek, F., Braeuer, G., & Muller, H. (1960). Molybdenum and niobium sulphides. *Nature 185*, 376-377. http://doi.org/10.1038/185376a0

Krebs, E., Silvi, B., & Raybaud, P. (2008). Mixed sites and promoter segregation: A *DFT* study of the manifestation of Le Chatelier's principle for the Co(Ni)MoS active phase in reaction conditions. *Catalysis Today 130*, 160-169. http://doi.org/10.1016/j.cattod.2007.06.081

Kurth, S., Perdew, J. P., & Blaha, P. (1999). Molecular and solid-state tests of density functional approximations: LSD, GGAs, and meta-GGAs. *International Journal of Quantum Chemistry 75*, 889-909. http://doi.org/10.1002/(SICI)1097-461X(1999)75:4/5<889::AID-QUA54>3.0.CO;2-8

Lauritsen, J. V., & Besenbacher, F. (2015). Atom-resolved scanning tunneling microscopy investigations of molecular adsorption on MoS_2 and $CoMoS$ hydrodesulfurization catalysts. *Journal of Catalysis 328*, 49-58. http://doi.org/10.1016/j.apcata.2004.10.012

Mohan, N., & Suresh, C. H. (2014). A molecular electrostatic potential analysis of hydrogen, halogen, and dihydrogen bonds. *The Journal of Physical Chemistry A 118*, 1697-1705. http://doi.org/10.1021/jp4115699

Monkhorst, H. J., & Pack, J. D. (1976). Special points for Brillouin-zone integrations. *Physical Review B 13*, 5188-5192. http://doi.org/10.1103/PhysRevB.13.5188

Okamoto, Y., Kawano, M., Kawabata, T., & Kubota, T. (2005). Structure of the active sites of Co-Mo hydrodesulfurization catalysts as studied by magnetic susceptibility measurement and NO adsorption. *Journal of Physical Chemistry B 109*, 288-296.

Perdew J. P, B. K., & Ernzerhof, M. (1996). Generalized gradient approximation made simple. *Physical Review Letters 77*, 3865-3868.

R. Romero, A., Ramírez, J., & Cedeño, L. (2003). Study of the activation and characterization of Mo on Nb modified alumina catalysts. *Revista Mexicana De Ingeniería Química 2*, 75-81.

Raybaud, P., Hafner, J., Kresse, G., Kasztelan, S., & Toulhoat, H. (2000). *Ab initio* study of the $H_2 - H_2S/MoS_2$ gas-solid interface: The nature of the catalytically active sites. *Journal of Catalysis 189*, 129-146. http://doi.org/10.1006/jcat.1999.2698

Reuter, K., & Scheffler, M. (2001). Composition, structure, and stability of RuO_2(100) as a function of oxygen pressu. *Physical Review B 65*, 035406. http://doi.org/10.1103/PhysRevB.65.035406

Reuter, K., & Scheffler, M. (2002). Composition, structure, and stability of RuO_2(110) as a function of oxygen pressure. *Physical Review B - Condensed Matter and Materials Physics 65*, 1-11. http://doi.org/10.1103/PhysRevB65.035406

Reuter, K., & Scheffler, M. (2003). First-principles atomistic thermodynamics for oxidation catalysis: Surface phase diagrams and catalytically interesting regions.

Physical Review Letters 90, 046103. http://doi.org/10.1103/PhysRevLett.90 .046103

Rogal, J., Reuter, K., & Scheffler, M. (2004). Thermodynamic stability of PdO surfaces. *Physical Review B 69*, 075421. http://doi.org/10.1103/PhysRevB.69.075421

Scrocco, E., & Tomasi, J. (1978). Electronic molecular structure, reactivity and intermolecular forces: An euristic interpretation by means of electrostatic molecular potentials. *Advances in Quantum Chemistry 11*, 115-193. http://doi.org/10.1016/S0065-3276(08)60236-1

Sjoberg, P., & Politzer, P. (1990). Use of the electrostatic potential at the molecular surface to interpret and predict nucleophilic processes. *The Journal of Physical Chemistry 94*, 3959-3961. http://doi.org/10.1021/j100373a017

Song, I., Park, C., & Choi, H. C. (2015). Synthesis and properties of molybdenum disulphide: from bulk to atomic layers. *RSC Advances 5*, 7495-7514. http://doi.org/10.1039/C4RA11852A

Theophilou, A. K., & Glushkov, V. (2005). *DFT* with effective potential expressed as a mapping of the external potential: Applications to closed-shell molecules. *International Journal of Quantum Chemistry 104*, 538-550. http://doi.org/10.1002/qua.20640

Torres, G. (2018). Preparation and evaluation of NiCoMo hydrodesulfurization catalysts supported over a binary zeolite(Beta)-Kit-6 siliceous material. *Revista Mexicana de Ingeniería Química 17*, 215-228. http://doi.org/10.24275/uam/izt/dcbi/revmexingquim/2018v17n1/torres

Ushikubo, T. (2000). Recent topics of research and development of catalysis by niobium and tantalum oxides. *Catalysis Today 57*, 331-338. http://doi.org/10.1016/S0920-5861(99)00344-2

Vogelaar, B. M., Kagami, N., van der Zijden, T. F., van Langeveld, A. D., Eijsbouts, S., & Moulijn, J. A. (2009). Relation between sulfur coordination of active sites and HDS activity for *Mo* and *NiMo* catalysts. *Journal of Molecular Catalysis A: Chemical 309*, 79-88. http://doi.org/10.1016/j.molcata.2009.04.018

Wang, T., Liu, X., Wang, S., Huo, C., Li, Y.-W., Wang, J., & Jiao, H. (2011). Stability of $\beta - Mo_2C$ facets from *ab initio* atomistic thermodynamics. *The Journal of Physical Chemistry C 115*, 22360-22368. http://doi.org/10.1021/jp205950x

Zhao, S., Liu, X.-W., Huo, C.-F., Li, Y.-W., Wang, J., & Jiao, H. (2012). Surface morphology of Hägg iron carbide ($\xi - Fe_5C_2$) from *ab initio* atomistic thermodynamics. *Journal of Catalysis 294*, 47-53. http://doi.org/10.1016/j.jcat.2012.07.003

Zhu, Y., Ramasse, Q. M., Brorson, M., Moses, P. G., Hansen, L. P., Topsøe, H., . . . Helveg, S. (2016). Location of Co and Ni promoter atoms in multi-layer MoS_2 nanocrystals for hydrotreating catalysis. *Catalysis Today 261*, 75-81. http://doi.org/10.1016/j.cattod.2015.08.053